

# Selected Applications of the Macroscopic-Microscopic Method

Kasia MAZUREK

Institute of Nuclear Physics  
Polish Academy of Sciences, Kraków, Poland

March 1, 2013

## Outline

- Macroscopic-Microscopic Method
  - a) Shell and Pairing Energies
  - b) Macroscopic Models
- Applications
  - a) Shape Coexistence
  - b) Islands of Inversion
  - c) Rotational Bands
  - d) Superdeformation
  - e) Giant Dipole Resonance
  - f) Fission Dynamics
- Summary

# Macroscopic-Microscopic Method

$$M(Z, N; def) = ZM_H + NM_n - 0.00001433Z^{2.39} \\ + E_{LSD}(Z, N; def) + E_{micr}(Z, N; def)$$

Macroscopic Energy: Lublin - Strasbourg Drop, Finite Range Liquid Drop Model Microscopic Energy

$$E_{micr} = E_{pair} + E_{shell}$$

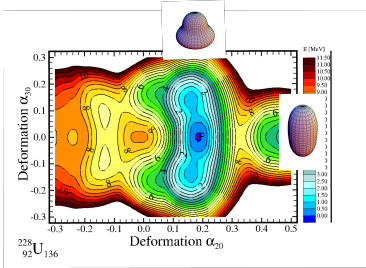
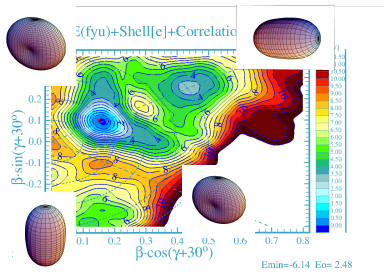
'Pairing' Energy

$$E_{pair} = E_{BCS} + \bar{E}_{pc}$$

# Macroscopic-Microscopic Method

Nuclear surface parametrization:

$$\mathcal{R}(\vartheta, \varphi) = R_0 c(\{\alpha\}) \sum_{\lambda, \mu} [1 + \alpha_{\lambda, \pm \mu} Y_{\lambda, \pm \mu}(\vartheta, \varphi)]$$



$$\{\beta, \gamma\} \rightarrow \{\alpha_{20}, \alpha_{22}\}$$

# Macroscopic-Microscopic Method

## Woods-Saxon Single-Particle Potential

[ S. Ćwiok, J. Dudek, W. Nazarewicz, J. Skalski, T. Werner, Comp. Phys Comm **46** (1987) 379 ]

$$\langle \nu | \mathbf{h}(1) | \mu \rangle = e_\nu \delta_{\nu\mu}$$

$$h(1) \Rightarrow \hat{H}_{WS} = \hat{t} + \hat{V}_{WS} \Rightarrow \hat{V}_{WS} = \hat{V}_{cent} + \hat{V}_{so} + \hat{V}_{Coul}$$

$$\hat{V}_{cent}(\vec{r}; V_0, \kappa, a, r_0) = \frac{V_0 \left[ 1 \pm \kappa \frac{N-Z}{N+Z} \right]}{\left\{ 1 + \exp \left[ \text{dist}_{\Sigma_0(\vec{r}, r_0)} / a \right] \right\}}; \quad V_{Coul} = \begin{cases} \frac{Ze^2}{r} \\ \frac{Ze^2}{2R_0} \left[ 3 - \left( \frac{r}{R_0} \right)^2 \right] \end{cases}$$

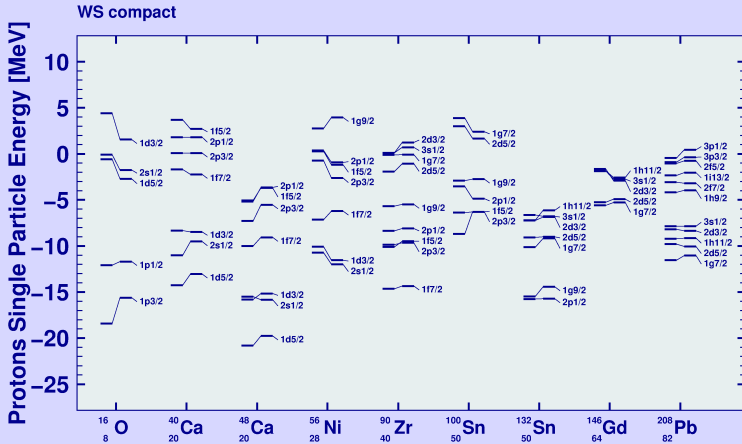
The spin-orbit term:

$$\hat{V}_{so}(\vec{r}, \vec{p}; V_0^{so}, \kappa, a_{so}, r_{so}) = \lambda \left[ \frac{\hbar}{2mc} \right]^2 \left[ \vec{\nabla} \frac{V_0^{so} \left[ 1 \pm \kappa \frac{N-Z}{N+Z} \right]}{1 + \exp \left[ \text{dist}_{\Sigma_{so}(\vec{r}, r_{so})} / a_{so} \right]} \right] \times \vec{p} \cdot \vec{s};$$

$$V_0^{so} = \lambda \left[ \frac{\hbar}{2mc} \right]^2 V_0 \left[ 1 \pm \kappa \frac{N-Z}{N+Z} \right]; \quad R_0 = r_0 A^{1/3}$$

## Macroscopic-Microscopic Method

## *Single-particle levels*



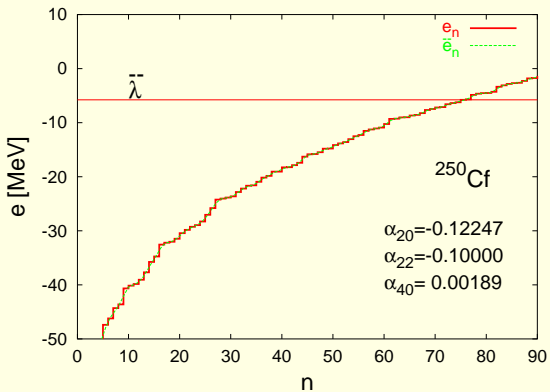
### Comparison of the calculated (right) and experimental (left) single-particle levels

- new UNIVERSAL-DIRAC parameters. (*PhD thesis of N. Dubray*)

# Macroscopic-Microscopic Method

## Strutinski Shell Energy

$$E_{shell} = \sum_{n=1}^N e_n - \int_0^N \bar{e}_n(n) dn$$



# Macroscopic-Microscopic Method

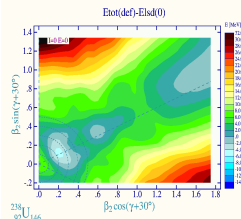
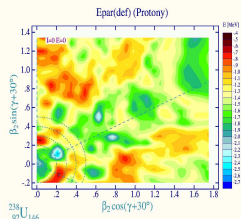
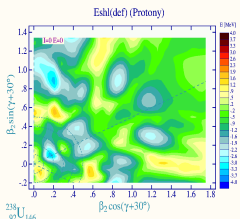
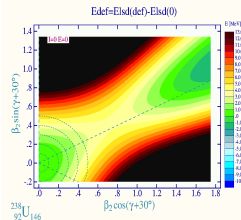
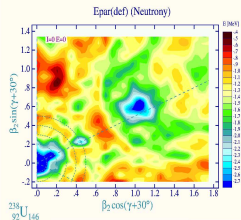
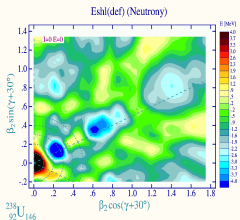
## Pairing Energy

$$E_{\text{pair}} = E_{\text{BCS}} + \bar{E}_{\text{pc}}$$

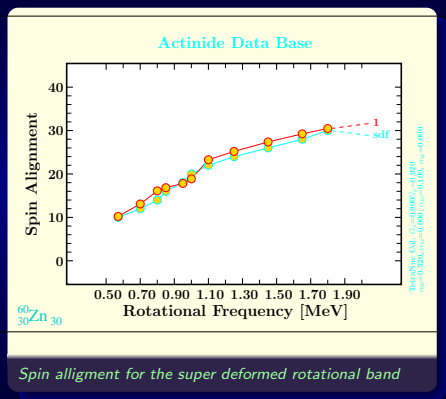
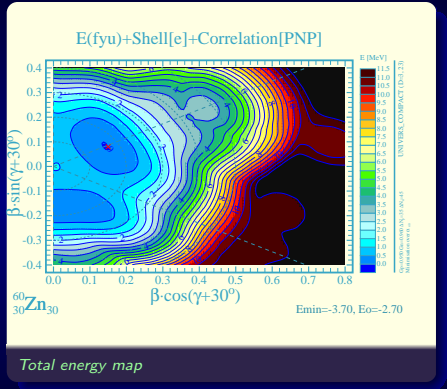
$$\begin{aligned} E_{\text{BCS}} &= \sum_{\nu=\mathcal{N}_1}^{\mathcal{N}_2} 2v_\nu^2(e_\nu - \lambda) - \frac{\Delta^2}{G} - G \left( \sum_{\nu=\mathcal{N}_1}^{\mathcal{N}_2} v_k^4 - \sum_{\nu=\mathcal{N}_1}^{\mathcal{N}_2} 1 \right) \\ &\quad - \sum_{\nu=\mathcal{N}_1}^{\mathcal{N}_2} (e_\nu - \lambda) \\ \bar{E}_{\text{pc}} &= -\frac{1}{4} \frac{N^2}{\rho} \left\{ \left[ 1 + \left( \frac{2\rho\Delta}{N} \right)^2 \right]^{1/2} - 1 \right\} + \frac{1}{2} \frac{\rho\Delta G}{2\rho\Delta} \arctan \frac{N}{2\rho\Delta} \end{aligned}$$

$$\Delta_n = 9.08/\sqrt{A}, \quad \Delta_p = 9.85/\sqrt{A}$$

# Macroscopic-Microscopic Method



# Macroscopic-Microscopic Method with Cranking



$$\hat{H}_{WS}^\omega = \hat{H}_{WS} - \omega \cdot \hat{j}$$

# Conclusions for the Macroscopic Models

- The nuclear surface energy comes from the nuclear matter contained in a certain surface region whose magnitude is determined by its diffusivity.

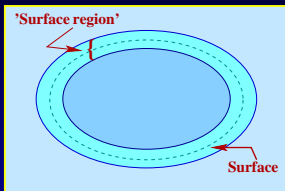


Figure: *For Steiner sheets and relatively thin skin (small surface region) the amount of nuclear matter contained in the surface region is approximately proportional to the volume of the surface region.*

- The volume of the 'surface region',  $\mathcal{V}_S$ , is approximated by

$$\mathcal{E}_{\text{surf}} \sim \mathcal{V}_S \sim \int_{S_1}^{S_2} \mathcal{S}(s) ds \sim \int_{S_1}^{S_2} [\mathcal{S}_0 + \mathcal{L}_0 s] ds$$

# Conclusions for the Structure of $\mathcal{E}_{surf}$

- The nuclear surface energy can be decomposed into at least two terms whose  $\mathbf{A}$ -dependences are different:  $\underline{\mathbf{A}^{2/3}}$  and  $\underline{\mathbf{A}^{1/3}}$
- At the same surface area  $\mathcal{S}_0$  two nuclei differing by average curvatures  $\mathcal{L}_0$  and  $\mathcal{L}'_0$ , will have different surface energies
- Since the proportionality coefficients  $\mathcal{C}_S(Z, N)$  and  $\mathcal{C}_L(Z, N)$  are in fact '*functions of the nucleus*', it follows that in two different nuclear regions the relative proportions of the surface-area term to the surface-curvature term will be in general different (e.g. vanishing surface-curvature)
- The surface energy is proportional to the *volume of the surface region*
- There is no *a priori* statement about the sign of curvature contributions

# The Physics of the Nuclear Surface

- The fit of parameters of the extended formula to 2772 masses improves the results for the barriers by better than a factor of 4 (!!)

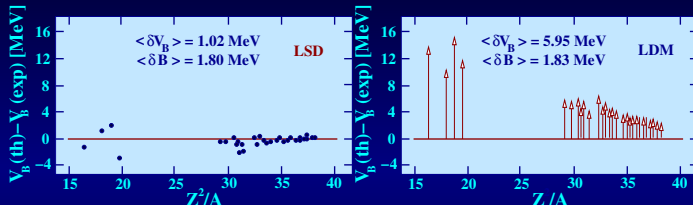


Figure: *Results of the fitting of the parameters to the experimental masses give simultaneously and improvement in the description of the experimental fission barriers (left); fit performed under the same conditions but without curvature terms ('traditional') is given for comparison on the right.*

K. Pomorski, J. Dudek, Phys. Rev. C 67,044316(2003)

## Macroscopic energy calculations

- In the past, often the Yukawa-folded approach has been used;
- In such an approach the surface energy is obtained through a procedure using the Yukawa-folding function  $F(|\vec{r} - \vec{r}'|, a)$

## Macroscopic energy calculations

- In the past, often the Yukawa-folded approach has been used;
- In such an approach the surface energy is obtained through a procedure using the Yukawa-folding function  $F(|\vec{r} - \vec{r}'|, a)$
- The diffuseness parameter  $a$  serves to collect the contributions from the nuclear surface region only

## Macroscopic energy calculations

- In the past, often the Yukawa-folded approach has been used;
- In such an approach the surface energy is obtained through a procedure using the Yukawa-folding function  $F(|\vec{r} - \vec{r}'|, a)$
- The diffuseness parameter  $a$  serves to collect the contributions from the nuclear surface region only
- The folding procedure results in a dangerous loss of sensitivity with respect to high-order multipoles

## Macroscopic energy calculations

- In the past, often the Yukawa-folded approach has been used;
- In such an approach the surface energy is obtained through a procedure using the Yukawa-folding function  $F(|\vec{r} - \vec{r}'|, a)$
- The diffuseness parameter  $a$  serves to collect the contributions from the nuclear surface region only
- The folding procedure results in a dangerous loss of sensitivity with respect to high-order multipoles
- Also the fission barrier-heights especially for the lighter nuclei do not correspond well with the experimental data

# The Final LSD Macroscopic Energy Expression

- Mass-fits are improved slightly with respect to other models but the fission barriers are improved considerably;
- The fission barriers involve large deformations where the curvature of the nuclear surface plays an important role;
- This significant improvement confirms the right physics:

$$\begin{aligned} E_{lsd}(Z, N; def) &= b_{vol}\{1 - \kappa_{vol}[(N - Z)/A]^2\} A \\ &+ b_{surf}\{1 - \kappa_{surf}[(N - Z)/A]^2\} A^{2/3} B_{surf}(def) \\ &+ b_{curv}\{1 - \kappa_{curv}[(N - Z)/A]^2\} A^{1/3} B_{curv}(def) \\ &+ \frac{3}{5} e^2 \frac{Z^2}{r_0^{ch} A^{1/3}} B_{Coul}(def) \\ &+ E_{micr}(Z, N; def) \\ &+ E_{cong}(Z, N; def) \end{aligned}$$

K. Pomorski, J. Dudek, Phys. Rev. C **67**, 044316(2003),

J. Dudek, K. Pomorski, N. Schunck, N. Dubray, Eur. Phys. J. A **20**, 15 (2004)

- At high temperatures, the total nuclear energy can be approximated by the macroscopic energy expression only
- The angular momentum effects can be treated, to the first approximation classically

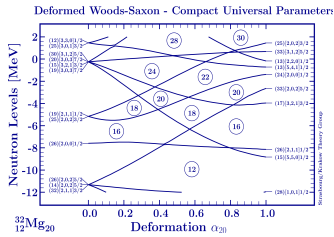
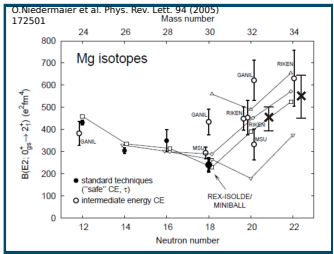
$$E_{\text{total}}(\{\text{def.}\}; I) = E_{\text{macro}}(\{\text{def.}\}) + \frac{\hbar^2}{2J\{\text{def.}\}} \cdot I(I+1)$$

- Conclusion:

Using the macroscopic energy as optimal as possible will be of importance: in our case → the LSD Model

# Applications → T=0, Spin=0

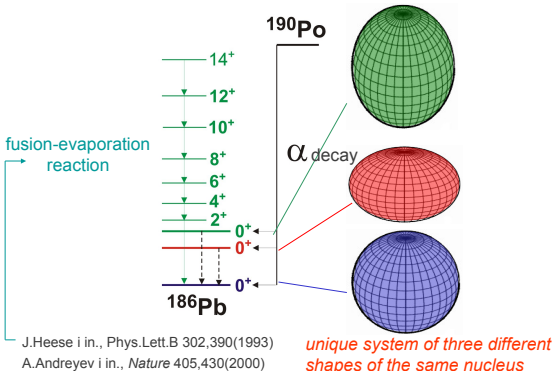
## Inversion Islands



# Applications → T=0, Low Spin

## Shape coexistence in the atomic nucleus

$$82 < N = 104 < 126$$



J.Heese i in., Phys.Lett.B 302,390(1993)

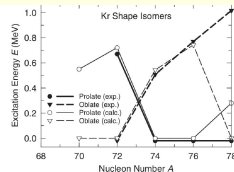
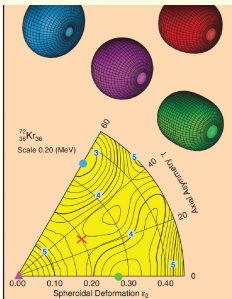
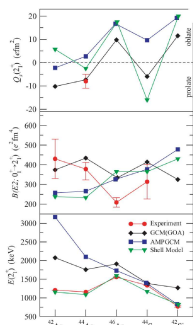
A.Andreyev i in., Nature 405,430(2000)

Courtesy of W. Meczynski

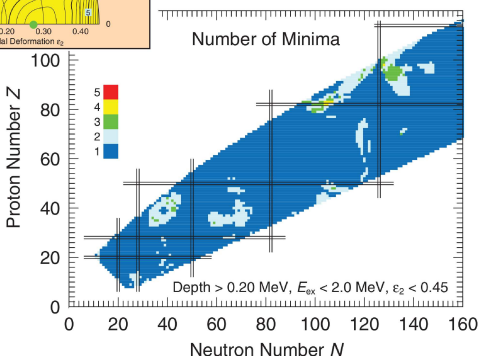
# Applications → T=0, Low Spin

## Shape coexistence

M. Zielińska et al.  
PHYSICAL REVIEW C 80, 014317 (2009)



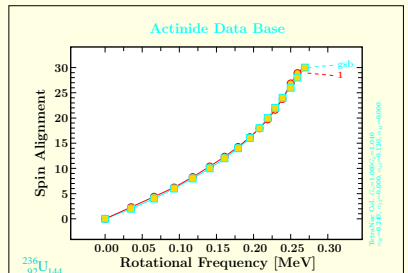
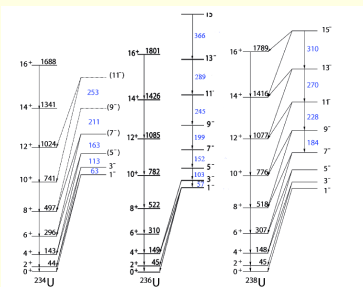
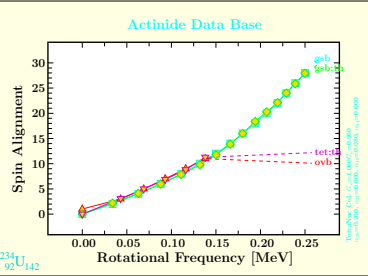
P. Moller PRL 103, 212501 (2009)



# Applications → T=0, Low Spin

## Rotational Bands- low spin

D. Curien et al. Phys. J. Phys. Conf. Ser. 205 (2010) 012034



# Applications → T=0, High Spin

## Superdeformation - $^{152}\text{Dy}$

J. Dudek et al., Eur. Phys. J. A 20 (2004) 165; H. Savajols et al., Phys. Rev. Lett. 76, 4480 (1996)

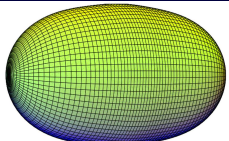
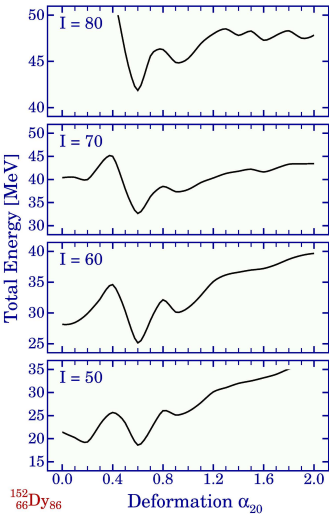
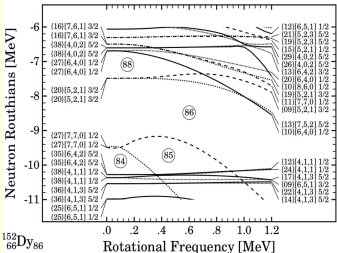


Fig. 1. The superdeformed nucleus  $^{152}\text{Dy}$ , according to the measurements of ref. [8] has the quadrupole moment  $Q_2 = 17.2$  eb. The corresponding deformation  $\alpha_{20} = 0.61$  and  $\alpha_{40} = 0.11$  obtained, e.g., from the calculations with the Woods-Saxon potential as in ref. [9] reproduces the measured dynamical moments and the quadrupole moment. The shape presented in the figure corresponds to the above deformation.



# Applications → T=0, High Spin/ Low spin

## Superdeformation

G. ROYER AND J. GAUDILLOT

PHYSICAL REVIEW C 84, 044602 (2011)

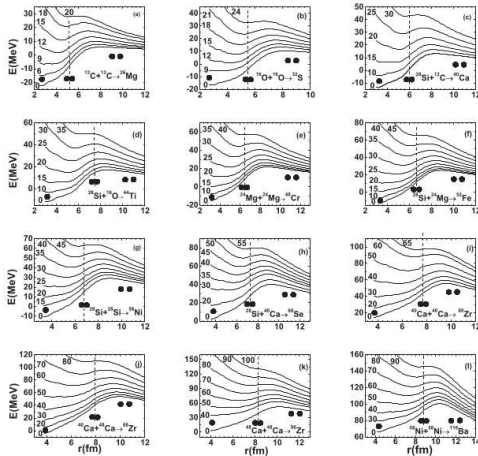


FIG. 1. Fusion barriers vs the angular momentum (in units of  $\hbar$ ) and the distance  $r$  between the mass centers for the  $^{12}\text{C} + ^{13}\text{C}$ ,  $^{16}\text{O} + ^{32}\text{S}$ ,  $^{28}\text{Si} + ^{32}\text{S}$ ,  $^{28}\text{Si} + ^{40}\text{Ca}$ ,  $^{28}\text{Si} + ^{40}\text{Mg}$ ,  $^{28}\text{Si} + ^{36}\text{S}$ ,  $^{40}\text{Ca} + ^{40}\text{Ca}$ ,  $^{40}\text{Ca} + ^{48}\text{Ca}$ ,  $^{48}\text{Ca} + ^{60}\text{Ca}$ , and  $^{58}\text{Ni} + ^{58}\text{Ni}$  nuclear systems. The dashed vertical line indicates the contact point between the spherical nuclei.

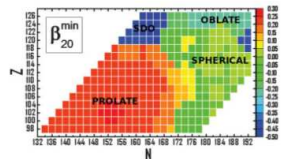


FIG. 1. (Color online) Calculated ground-state quadrupole deformations  $\beta_{20}$ .

P. JACHIMOWICZ, M. KOWAL, AND J. SKALSKI

PHYSICAL REVIEW C 83, 054302 (2011)

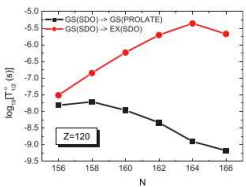


FIG. 4. (Color online) Calculated  $\log_{10}(T_{1/2}^g \text{ [s]})$  values for g.s. to g.s. (the lower line) and g.s. to SDO (the upper line)  $\alpha$  decays of  $Z = 120$  neutron-deficient nuclei.

# Applications → T=0, No Spin

## Low-Energy Shape Oscillations

### Low-energy shape oscillations of negative parity

M. KOWAL AND J. SKALSKI  
PHYSICAL REVIEW C 82, 054303 (2010)

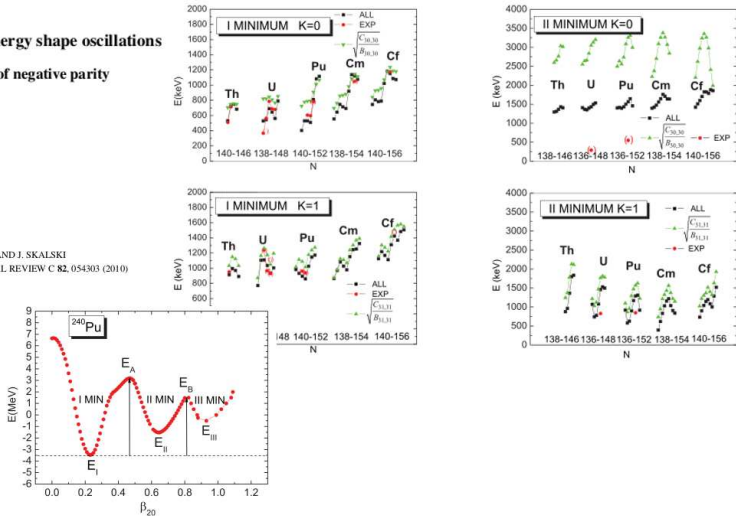
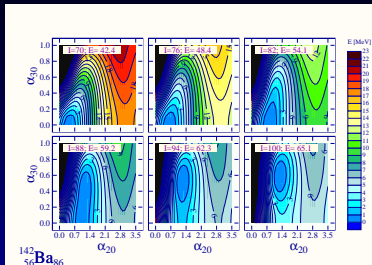


FIG. 1. (Color online) Calculated fission barrier for  $^{240}\text{Pu}$  as a function of  $\beta_{20}$ .



# Collective Hamiltonian.



## Octupole vibration

(<http://oer.physics.manchester.ac.uk/NP/Collective/l3.html>)

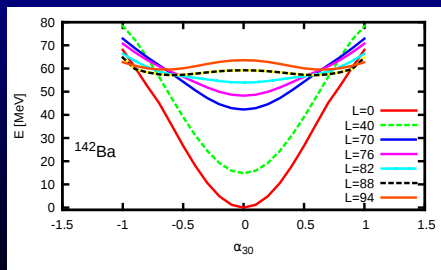
$$\hat{H} = \frac{\hbar^2}{2B} \frac{\delta^2}{\delta \alpha_{30}^2} + \frac{1}{2} C \alpha_{30}^2$$

where  $B$  is the mass parameter and  $C$  the stiffness of the potential.

$$\langle \psi_n | \hat{H} | \psi_m \rangle = e_n \delta_{nm}$$

$$\hat{H} = \frac{\hbar^2}{2B} \frac{\delta^2}{\delta \alpha_{30}^2} + V(\alpha_{30})$$

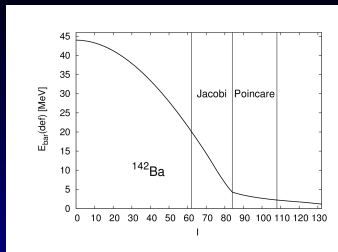
A. Bohr, B. Mottelson, Nuclear Structure vol. II



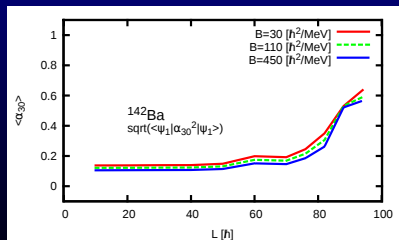
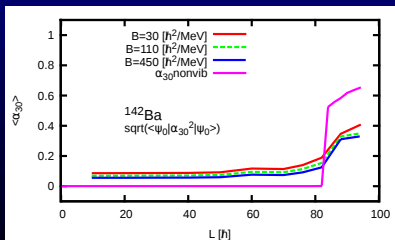
# Collective hamiltonian.

The first  $1^-$  state is usually described as 0 - point motion vibration. For  $^{142}\text{Ba}$  the energy of this level is 1.326 MeV.

$\hbar\omega$ [MeV]	B [ $\hbar^2/\text{MeV}$ ]	$e_0$ [MeV]
0.5	30	1.89
1.0	110	1.48
1.5	450	1.2



The mean values of the dynamical octupole deformation of  
0 - state excitation -  $\sqrt{\langle \psi_0 | \alpha_{30}^2 | \psi_0 \rangle}$       1 - state excitation -  $\sqrt{\langle \psi_1 | \alpha_{30}^2 | \psi_1 \rangle}$

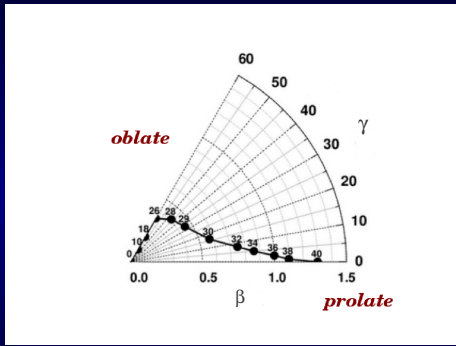
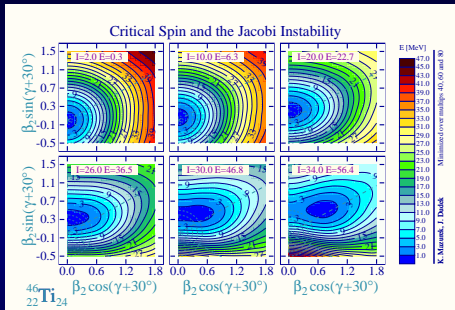


K.M., J. Dudek, A. Maj, submitted to PRC

# Applications $\rightarrow T \neq 0$ , High Spin

## Giant Dipole Resonances-Jacobi Shape Transition.

Total energy minimum evolution with increasing the spin -  $^{46}\text{Ti}$ .



## Spherical - oblate - nonaxial - prolate

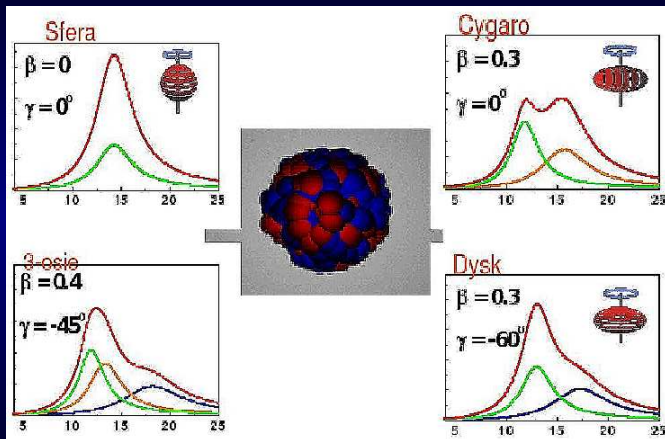
A. Maj et al., Nucl. Phys. **A 731**, 319 (2004)

M. Kmiecik et al., Phys. Rev. **C 70**, 064317 (2004)

N. Schunck et al., Phys. Rev. **C 75**, 054304 (2007)

# Applications $\rightarrow T \neq 0$ , High Spin

## Giant Dipole Resonances



The shape evolution of the compound nucleus influents into the GDR strength function. A. Maj et al., Nucl. Phys. A 731, 319 (2004)

# Applications $\rightarrow T \neq 0$ , High Spin

## Giant Dipole Resonances

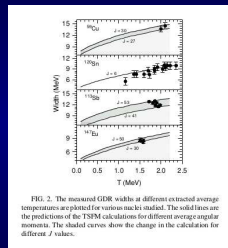
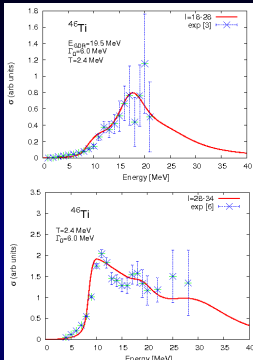
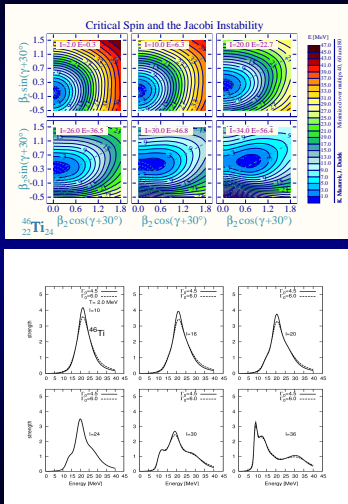


FIG. 2. The measured GDR widths at different extracted average temperatures are plotted for various nuclei studied. The solid lines are the predictions of the TSM calculations for different average angular momenta. The shaded curves show the change in the calculation for different  $J$  values.

Eksperiment: A. Maj et al.,

Nucl. Phys. A 731, 319 (2004).

S. Bhattacharya et al., PRC 78,

064601 (2008)

# Applications → T ≠ 0, High Spin

*Fission dynamics-Langevin equations*

$$\frac{dq_i}{dt} = \sum_j [M^{-1}(\vec{q})]_{ij} p_j$$

$$\frac{dp_i}{dt} = -\frac{1}{2} \sum_{j,k} \frac{d[M^{-1}(\vec{q})]_{jk}}{dq_i} p_j p_k - \frac{dV(\vec{q})}{dq_i} - \sum_{j,k} \gamma_{ij}(\vec{q}) [M^{-1}(\vec{q})]_{jk} p_k + \sum_j g_{ij}(\vec{q}) \Gamma_j$$

- $[M^{-1}(\vec{q})]_{ij}$  - tensor of inertia,  $M_{ij}$  - tensor of mass
- $V(\vec{q})$  - potential energy
- $\vec{q} = (q_1, q_2, q_3)$  - collective coordinates
- $\vec{p} = (p_1, p_2, p_3)$  - conjugate momenta
- $\Gamma_j(t)$  - random variable:  $\langle \Gamma_i \rangle = 0$ ,  $\langle \Gamma_i(t_1) \Gamma_j(t_2) \rangle = 2\delta_{ij}\delta(t_1 - t_2)$
- $D_{ij} = g_{ik}g_{kj} \equiv T\gamma_{ij}$  - diffusion tensor
- $T = [E_{int}/a(\vec{q})]^{1/2}$  - temperature from Fermi gas model
- $E_{int}$  - internal excitation energy
- $E_{coll}(\vec{q}, \vec{p}) = \frac{1}{2}[M^{-1}(\vec{q})]_{ij} p_i p_j$  - the kinetic energy of the collective degrees of freedom
- $a(\vec{q}) = a_v A + a_s A^{2/3} B_s(\vec{q})$  - Ignatyuk level density parameter

# Applications

Collective coordinates in “funny hills” parametrisation

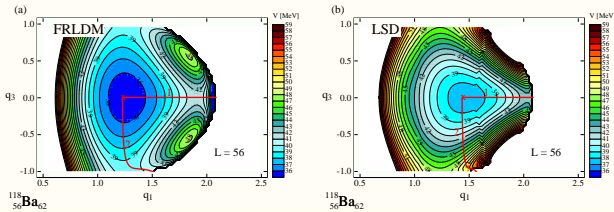
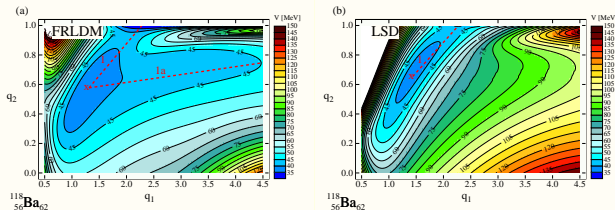
$$\begin{aligned} q_1 &= c \\ q_2 &= \frac{h+3/2}{\frac{5}{2c^3} + \frac{1-c}{4} + 3/2} \\ q_3 &= \begin{cases} \alpha/(A_s + B), & B \geq 0 \\ \alpha/A_s, & B \leq 0 \end{cases} \end{aligned}$$

$$\rho_s^2(z) = \begin{cases} (c^2 - z^2)(A_s + Bz^2/c^2 + \frac{\alpha z}{c}), & B \geq 0 \\ (c^2 - z^2)(A_s + \frac{\alpha z}{c}) \exp(Bzc^2), & B \leq 0 \end{cases}$$

$$B = 2h + \frac{c-1}{2}$$
$$A_s = \begin{cases} c^{-3} - \frac{B}{5}, & B \geq 0; \\ -\frac{4}{3} \frac{B}{\exp(Bc^3) + (1 + \frac{1}{2Bc^3}) \sqrt{-\pi Bc^3} \operatorname{erf}(\sqrt{-Bc^3})}, & B \leq 0 \end{cases}$$

# Applications

## Potential Energy Surfaces (PES)

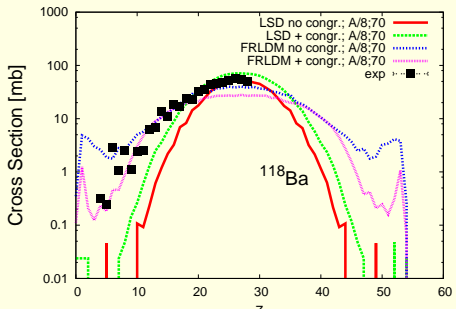


The potential energy surfaces for the  $^{118}\text{Ba}$  calculated with the LSD (right) and the FRLDM model (left) in the plane  $(q_1, q_2)$ -top and  $(q_1, q_3)$ -bottom.

# Applications

## FF Charge distribution

G. Ademard et al., Phys. Rev. C 83, 054619 (2011)



*Z distribution for  $^{118}\text{Ba}$  with angular momentum  $l = 0 - 70 \hbar$  for potential energy surfaces calculated with the LSD formula and FRLDM model and with constant density parameter  $a=A/8$  with viscosity  $k_s = 0.2$ . The influence of the congruence (Wigner) energy is shown.*

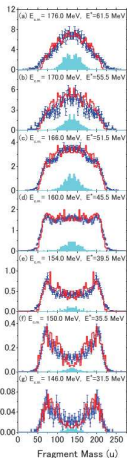
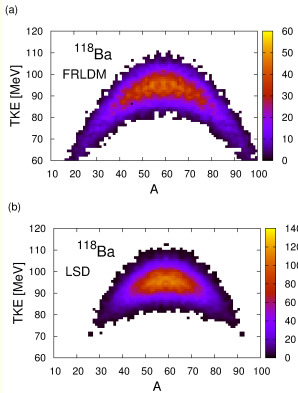


FIG. 4. (Color online) Mass distributions of fission fragments for the reaction of  $^{34}\text{S} + ^{238}\text{U}$ . The experimental data and the calculated result are denoted by the circles [15] and the histogram, respectively. The shaded areas show the calculated fusion-fission events.

Y. Aritomo et al. PRC

# Applications



Correlation between the mass  $A$  and total kinetic energy TKE of the fission fragments produced in the reaction  $^{78}\text{Kr}(429 \text{ MeV}) + ^{40}\text{Ca} \rightarrow ^{118}\text{Ba}$ . The top (bottom) panel shows the calculation performed with the FRLDM (LSD) potential. In all calculations, the level-density parameter is  $a = A/8 \text{ MeV}^{-1}$  and  $k_s$  is set to 0.2.

## FRLDM LSD

	FRLDM	LSD
$P_f$	<b>0.42</b>	<b>0.49</b>
$\langle n_{pre} \rangle$	<b>0.03</b>	<b>0.03</b>
$\langle p_{pre} \rangle$	<b>0.06</b>	<b>0.04</b>
$\langle \alpha_{pre} \rangle$	<b>0.03</b>	<b>0.03</b>
$\langle n_{eva} \rangle$	<b>1.31</b>	<b>1.38</b>
$\langle p_{eva} \rangle$	<b>3.00</b>	<b>3.09</b>
$\langle \alpha_{eva} \rangle$	<b>1.47</b>	<b>1.43</b>
$\sigma_A^2$	<b>371.86</b>	<b>126.13</b>
$\sigma_Z^2$	<b>83.82</b>	<b>28.69</b>
$\langle TKE \rangle$	<b>87.48</b>	<b>94.17</b>
$\sigma_{E_k}^2$	<b>197.13</b>	<b>35.83</b>
$\langle T_{sc} \rangle$	<b>1.67</b>	<b>1.68</b>

K. M., C. Schmitt, J.P. Wileczko, P.N. Nadtochy, G. Ademard, Phys. Rev. C 84, 014610 (2011)

## Summary and Conclusions

- *The MMM is very powerful method to estimate many experimental observables*
- *The nuclear shape deformation is easy investigated within this method*
- *The description of cold and excited nuclei can be done with reasonable precision*
- *The rotational bands and low-energy excitation can be also reproduced*

# Last years and Macroscopic-Microscopic Method in Phys. Rev. C:

- Deformation in  $^{28}Si^*$  produced via the  $^{16}O + ^{12}C$  reaction, *PhysRevC* 87, 024602 (2013)
- Calculation of fission probability using one- and two-body dissipation in fusion-fission reactions *PhysRevC* 86, 044609 (2012)
- Fission barriers and half-lives of actinides in the quasimolecular shape valley, *PhysRevC* 86, 044326 (2012)
- Microscopic-macroscopic approach for binding energies with the Wigner-Kirkwood method. II. Deformed nuclei, *PhysRevC* 86, 044316 (2012)
- Effects of medium on nuclear properties in multifragmentation, *PhysRevC* 86, 024606 (2012)
- Predictions of the fusion-by-diffusion model for the synthesis cross sections of  $Z = 114\text{--}120$  elements based on macroscopic-microscopic fission barriers, *PhysRevC* 86, 014611 (2012)
- Four-dimensional Langevin dynamics of heavy-ion-induced fission, *PhysRevC* 85, 064619 (2012)
- Rotational states and masses of heavy and superheavy nucle, *PhysRevC* 84, 044310 (2011)
- Dynamical model of surrogate reactions, *PhysRevC* 84, 024602 (2011)
- Behavior of one-quasiparticle levels in odd isotonic chains of heavy nuclei, *PhysRevC* 84, 024324 (2011)
- Curvature effect on nuclear  $\hat{\alpha}$ pasta $\hat{\alpha}$ : Is it helpful for gyroid appearance?, *PhysRevC* 83, 065811 (2011)
- Surface symmetry energy of nuclear energy density functionals, *PhysRevC* 83, 034305 (2011)